

# Numerical Examination of a Squeezing Casson Hybrid Nanofluid Flow Considering Thermophoretic and Internal Heating Mechanisms

AMINE EL HARFOUF<sup>1,\*</sup>, RACHID HERBAZI<sup>2,3,4</sup>, WALID ABOULOIFA<sup>1</sup>,  
SANAA HAYANI MOUNIR<sup>1</sup>, HASSANE MES-ADI<sup>5</sup>, ABDERRAHIM WAKIF<sup>6</sup>,  
MOHAMED MEJDAL<sup>1</sup>, MOHAMED NFAOUI<sup>1</sup>

<sup>1</sup>Multidisciplinary Laboratory of Research and Innovation (LaMRI),  
Energy, Materials, Atomic and Information Fusion (EMAFI) Team,  
Polydisciplinary Faculty of Khouribga,  
Sultan Moulay Slimane University,  
MOROCCO

<sup>2</sup>Intelligent Systems and Applications Laboratory (LSIA), EMSI,  
Tangier,  
MOROCCO

<sup>3</sup>ENSAT, Abdelmalek Essaâdi University,  
Tangier,  
MOROCCO

<sup>4</sup>ERCMN, FSTT, Abdelmalek Essaâdi University,  
Tangier,  
MOROCCO

<sup>5</sup>Laboratory of Process Engineering, Computer Science and Mathematics,  
National School of Applied Sciences of the Khouribga University of Sultan Moulay Slimane,  
MOROCCO

<sup>6</sup>Faculty of Sciences Ain Chock, Laboratory of Mechanics,  
Hassan II University,  
Casablanca,  
MOROCCO

*\*Corresponding Author*

**Abstract:** - One of the main areas of study in the field is increasingly the flow of non-Newtonian fluids. These liquids find extensive use in nuclear reactors, food processing, paint and adhesives, drilling rigs, and cooling systems, among other industrial and engineering domains. However, hybrid nanofluids are crucial to the process of heat transfer. Considering this, this study investigates the motion of a Casson hybrid nanofluid squeezing flow between two parallel plates under the influence of a heat source and thermophoretic particle deposition. The Runge–Kutta–Fehlberg fourth–fifth-order approach is utilized to numerically solve the ordinary differential equations derived from the partial differential equations governing fluid flow, by utilizing suitable similarity variables. The diagrams show how several important parameters affect fluid profiles both with and without the Casson parameter. These figures demonstrate how fluid velocity increases as the local porosity parameter increases. When the heat source/sink parameter is increased, thermal dispersal increases, and when the thermophoretic parameter is increased, the concentration profile increases.

**Key-Words:** - Casson fluid, heat source/sink, hybrid nanofluid, parallel plates, thermophoretic particle deposition, The Runge–Kutta, non-Newtonian fluids.

Received: May 9, 2023. Revised: February 8, 2024. Accepted: March 6, 2024. Published: April 22, 2024.

## 1 Introduction

The nanofluid, which is a novel sort of heat transfer fluid, is created by suspending a single type of oxide and metallic nanoparticles, as well as nonmetallic carbon nanotubes, in carrier liquids including water, ethylene glycol, and oil, with a size of less than  $100\text{ nm}$  ( $C_2H_6O_2$ ). In comparison to heat transfer liquids, the nanofluid created by the solid nanoparticles suspended in the base liquids would have a higher thermal conductivity. These solid nanoparticles also possess favorable thermophysical properties. Additionally, nanofluids are widely used in a wide range of industrial and biomedical processes, including the production of glass fiber, metal spinning, the removal of tumors that cause hyperthermia, lubricant, the treatment of asthma, cable drawing, electronic devices, nuclear reactors, immunological synergy, chilling process, transportation, and power generation. Because of this, many researchers are interested in studying the flow of nanofluids over various geometries when various physical and chemical processes are present. The notion of nanofluid was first introduced in [1], who also illustrated the physical characteristics of nanoparticles. The stagnation point stream of nanofluid across a stretching cylinder was investigated by [2]. A study on the effect of activation energy in the presence of a fluid stream and the suspension of nanoparticles [3]. However, nanofluids were unable to provide the high heat transfer rate that large-scale manufacturing companies demanded, and this is where the heat transfer process became extremely complex.

To overcome this limitation, hybrid nanofluids are used instead of fluid suspended with single-kind nanoparticles. Different forms of liquids are produced when numerous kinds of minute nanoparticles come together to form hybrid nanofluids. These fluids are used in solar energy storage applications, the automotive industry, brake fluids for vehicles, and tubular heat exchangers. The numerical simulation of a water-based hybrid nanofluid flow over a curved stretching sheet, considering the Newtonian heating effect, was recently explained in [4]. Through an annulus, [5] examined the effects of radiation on the hybrid nanofluid stream. Information on the hybrid nanofluid stream passing through a cylinder [6]. [7] discussed the impact of slippage on a water-based hybrid nanofluid stream flowing across a curved surface. Recently, examination of how hybrid nanofluid flow behaves when it passes over an elastic sheet [8].

One important component of a liquid's flow across a media is its fluid rheology, which may be divided into two primary classes: Newtonian and non-Newtonian. The essential qualification between the non-Newtonian and Newtonian fluid models is the utilitarian relationship between shear push and shear rate. In differentiating to non-Newtonian fluids, Newtonian fluids don't show abdicating push. These fluids are widely used in nuclear reactors, food processing, paint and adhesives, drilling rigs, and cooling systems, among other industrial and engineering domains. One of the most significant rheological non-Newtonian fluid models used in the production of biological fluids, paints, and pharmaceuticals is the Casson fluid. Casson fluid is widely used in the drilling, food processing, and metallurgy industries, which makes rheological research on it crucial.

The authors in [9] investigated the MHD flow of nanofluids between parallel plates. The investigation of the incompressible flow of a nanofluid between parallel plates using ohmic heating settings was also explored [10]. Thermophoresis is the transfer of tiny particles from a high-temperature to a low-temperature environment. This phenomenon has various practical applications, such as following the trajectories of exhaust gas particles from burning devices, collecting microscopic particles from gas flows, and studying the deposition of particulate matter on turbine blades. Several scholars have investigated this phenomenon over the previous few decades, taking into consideration various biological repercussions. The authors [11] examined the thermophoretic deposition of aerosol particles on a liquid stream passing over a cylinder. [12] wrote about particle deposition on the axial stream of liquid over a cylinder. In literature [13]. Investigated the key aspects of thermophoretic particle deposition and the Soret-Dufour impact on the fluid stream over a revolving disk.

The research cited above leads one to the conclusion that there hasn't been much discussion of Casson hybrid nanofluid flow between two parallel plates in the presence of particle deposition and a heat source or sink. Therefore, under the influence of thermophoretic particle deposition and a heat source or sink, the stream of non-Newtonian Casson liquid containing hybrid ferrite nanoparticles  $NiZnFe_2O_4 - MnZnFe_2O_4$  between two parallel plates is examined in this work.

## 2 Problem Description and Formulation Mathematics

Here, we study the time-dependent flow of a Casson hybrid nanofluid between two parallel horizontal plates. Two ferrite nanoparticles,  $NiZnFe_2O_4 - MnZnFe_2O_4$ , are added to the base liquid,  $C_2H_6O_2$ , to create the hybrid nanofluid. Together, the plates and liquid rotate at an angular velocity along the y-axis, which is normal to the plates (Figure 1). The upper plate is located at  $y = h(t) = \pm l(1 - \alpha t)$  and the subordinate plate is positioned at  $y = 0$ , where it is stretched by two opposing and equal forces. Where the initial location (at time  $t = 0$ ) is indicated by  $l$ . When  $\alpha > 0$ , the plates are compressed until  $t = 1/\alpha$ , and when  $\alpha < 0$ , the two plates are separated. As a result, the point  $(0,0,0)$  stays in the same place. The governing equations are given below with these observations:

$$\frac{\partial u}{\partial x} + \frac{\partial v}{\partial y} = 0 \quad (1)$$

$$\frac{\partial u}{\partial t} + u \frac{\partial u}{\partial x} + v \frac{\partial u}{\partial y} = -\frac{1}{\rho_{hnf}} \frac{\partial P}{\partial x} + \frac{\mu_{hnf}}{\rho_{hnf}} \left(1 + \frac{1}{\beta}\right) \left(\frac{\partial^2 u}{\partial x^2} + \frac{\partial^2 u}{\partial y^2}\right) \quad (2)$$

$$\frac{\partial v}{\partial t} + u \frac{\partial v}{\partial x} + v \frac{\partial v}{\partial y} = -\frac{1}{\rho_{hnf}} \frac{\partial P}{\partial y} + \frac{\mu_{hnf}}{\rho_{hnf}} \left(1 + \frac{1}{\beta}\right) \left(\frac{\partial^2 v}{\partial x^2} + \frac{\partial^2 v}{\partial y^2}\right) \quad (3)$$

$$\left(\frac{\partial T}{\partial t} + u \frac{\partial T}{\partial x} + v \frac{\partial T}{\partial y}\right) = \frac{k_{hnf}}{(\rho c_p)_{hnf}} \left(\frac{\partial^2 T}{\partial x^2} + \frac{\partial^2 T}{\partial y^2}\right) + \frac{Q_0}{(\rho c_p)_{hnf}} T \quad (4)$$

$$\left(\frac{\partial C}{\partial t} + u \frac{\partial C}{\partial x} + v \frac{\partial C}{\partial y}\right) = D_{hnf} \left(\frac{\partial^2 C}{\partial x^2} + \frac{\partial^2 C}{\partial y^2}\right) - \frac{\partial(U_T C)}{\partial y} \quad (5)$$

The following are the related boundary conditions:

$$\begin{aligned} \frac{\partial u}{\partial y} \Big|_{y=0} &= 0, v \Big|_{y=0} = 0, \frac{\partial T}{\partial y} \Big|_{y=0} = 0, u \Big|_{y=h(t)} \\ &= 0, \\ v \Big|_{y=h(t)} &= v_w = \frac{dh}{dt}, T \Big|_{y=h(t)} = T_H \\ C \Big|_{y=h(t)} &= 0, \frac{\partial C}{\partial y} \Big|_{y=0} = 0 \end{aligned} \quad (6)$$

Thermophoretic velocity is given by  $U_T = -\frac{K v_f}{T_r} \frac{\partial T}{\partial y}$ , here,  $T_r$  is reference temperature and  $K$  is thermophoretic coefficient.

The similarity variables are mentioned below:

$$\begin{aligned} \eta &= \frac{y}{[l(1 - \alpha t)^{\frac{1}{2}}]} = \frac{y}{h(t)}, u \\ &= \frac{x\alpha}{2(1 - \alpha t)} f'(\eta), \\ v &= -\frac{\alpha l}{2(1 - \alpha t)^{\frac{1}{2}}} f(\eta), \theta = \frac{T}{T_H}, \phi = \frac{C}{C_H} \end{aligned} \quad (7)$$

Equation (7) can be substituted into Equations (2) and (3), and the pressure gradient can then be removed from the resultant equations to get:

$$\begin{aligned} \left(1 + \frac{1}{\beta}\right) f'''' + S(1 - \varphi_1)^{2.5} (1 \\ - \varphi_2)^{2.5} \left[ \left\{ (1 - \varphi_1) \right. \right. \\ \left. \left. + \frac{\rho_{S1}}{\rho_f} \varphi_1 \right\} (1 - \varphi_2) \right. \\ \left. + \frac{\rho_{S2}}{\rho_f} \varphi_2 \right] (f f'''' - 3f'' \\ - \eta f'''' - f' f'') = 0 \end{aligned} \quad (8)$$

Equation (7) helps to reduce the equations from (4) to (5). The following are the converted ordinary differential equations (ODEs):

$$\begin{aligned} \frac{k_{hnf}}{k_f} \theta'' + SP_r \left[ \left\{ (1 - \varphi_1) + \frac{\rho_{S1} C_{pS1}}{\rho_f C_f} \varphi_1 \right\} (1 \right. \\ \left. - \varphi_2) + \frac{\rho_{S2} C_{pS2}}{\rho_f C_f} \varphi_2 \right] (f \theta' \\ - \eta \theta') + Hs \theta \\ (1 - \varphi_1)^{2.5} (1 - \varphi_2)^{2.5} \phi'' + Sc S \phi' (f - \eta) \\ - \tau Sc (\theta'' \phi + \theta' \phi') \end{aligned} \quad (9)$$

Here are the diminished boundary conditions:

$$\begin{aligned} f''(0) = 0, f(0) = 0, \theta'(0) = 0, \phi'(0) \\ = 0 \quad \text{at} \quad \eta = 0 \\ f'(1) = 0, f(1) = 1, \theta(1) = 1, \phi(1) \\ = 1 \quad \text{at} \quad \eta = 1 \end{aligned} \quad (11)$$

Here  $S = \frac{\alpha l^2}{2\nu_f}$  is the squeeze number,  $P_r = \frac{\mu_f c_p f}{k_f}$  is the Prandtl number,  $H_s = \frac{l^2 Q_0}{k_f}$  is the heat source parameter  $Sc = \frac{\nu_f}{D_f}$  is Schmidt number,  $\tau = -\frac{K}{T_r}(T_w - T_H)$  is thermophoretic parameter. The following gives the thermophysical properties:

$$\frac{\mu_{hnf}}{\mu_f} = \frac{1}{(1 - \phi_1)^{2.5}(1 - \phi_2)^{2.5}}$$

$$(\rho c_p)_{hnf} = \left[ (1 - \phi_1)(1 - \phi_2) + \phi_2 \left( \frac{(\rho c_p)_{S2}}{(\rho c_p)_f} \right) + \phi_1 \left( \frac{(\rho c_p)_{S1}}{(\rho c_p)_f} \right) \right] (\rho c_p)_f \quad (12)$$

$$\frac{\rho_{hnf}}{\rho_f} = (1 - \phi_2) \left[ 1 - \left( 1 - \frac{\rho_{S1}}{\rho_f} \phi_1 \right) \right] + \phi_2 \frac{\rho_{S2}}{\rho_f}$$

$$k_{hnf} = k_f \left[ \frac{k_{S1} + 2k_f - 2\phi_1(k_f - k_{S1})}{k_{S1} + 2k_f + 2\phi_1(\lambda_f - k_{S1})} \right] \left[ \frac{k_{S2} + 2k_f - 2\phi_1(k_f - k_{S2})}{k_{S2} + 2k_f + 2\phi_1(k_f - k_{S2})} \right]$$

$$Cf = \left( 1 + \frac{1}{\beta} \right) \frac{\mu_{hnf}}{\rho_f \nu_w^2} \frac{\partial u}{\partial y} \Big|_{y=h(t)}$$

$$Sh = - \left( \frac{D_{hnf}}{D_f T_H} \right) \frac{\partial C}{\partial y} \Big|_{y=h(t)} \quad (13)$$

$$Nu = - \left( \frac{k_{hnf}}{k_f(T_w - T_H)} \right) \frac{\partial T}{\partial y} \Big|_{y=h(t)}$$

### 3 Outcome and Discussion

This section includes a brief explanation for better comprehension as well as a graphic representation of the nature of fluid profiles for several relevant parameters. For both the Casson hybrid nanoliquid

Equation (7) and (12) are used to reduce Equation (13)

$$c_f = \left| \frac{\left( 1 + \frac{1}{\beta} \right) f''(1)}{(1 - \phi_1)^{2.5}(1 - \phi_2)^{2.5}} \right| \quad (14)$$

$$Nu = \left| \frac{k_{hnf}}{k_f} \theta'(1) \right|$$

$$N_u = |(1 - \phi_1)^{2.5}(1 - \phi_2)^{2.5} \phi'(1)|$$

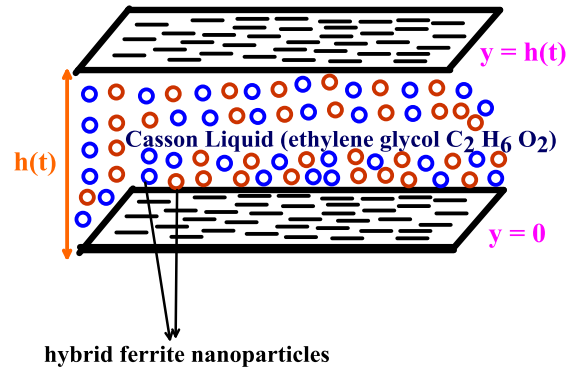


Fig 1: Geometry of the physical problem.

The definitions of the skin friction coefficient, Sherwood number, and Nusselt number are as follows:

$(\beta = 1.5)$  and the hybrid nanoliquid ( $\beta \rightarrow \infty$ ), the key effects of the porosity parameter, squeezing number, heat source or sink parameter, and thermophoretic parameter on fluid profiles are covered in detail. Graphs are also used to assess the fluctuation in the rate of mass and heat transfer. Table 1 lists the thermophysical characteristics of the nanoparticles  $NiZnFe_2O_4$ ,  $MnZnFe_2O_4$ , and  $C_2H_6O_2$ . By applying the appropriate similarity transformations, the flow's governing equations are converted into ODEs. Using the Runge–Kutta–Fehlberg fourth–fifth order (RKF 45) approach, a transformed collection of ODEs are solved. To validate the current result  $-f''(1)$ , Table 2 is produced using the published outcomes of [14]. when  $\phi_1$ ,  $\phi_2$  and  $\beta$  are not present.

The velocity profile  $f'(\eta)$  is shown in Figure 2 for a range of squeezing number  $S$  values. This graph shows that, for both  $\beta = 1.5$  and  $\beta \rightarrow \infty$ ,  $f'(\eta)$  dramatically decreases with increased values of  $S$  for  $\eta < 0.5$  and rises noticeably for  $\eta > 0.5$ .

Table 1. Thermophysical properties of  $NiZnFe_2O_4$ ,  $MnZnFe_2O_4$ , and  $C_2H_6O_2$

Particles	$\rho$ (kg/m <sup>3</sup> )	$C_p$ (J/kg K)	$k$ (W/m K)
$NiZnFe_2O_4$	4800	710	6.3
$MnZnFe_2O_4$	4700	1050	3.9
$C_2H_6O_2$	1116.6	2382	0.249

Table 2. Validation of the problem with existing work of, [14]. for different values of  $S$  when  $\varphi_1 = \varphi_2 = 0$  and  $\beta \rightarrow \infty$

Squeezing number $S$	$-f''(1)$	
	Ref [14]	Current results
-1.0	2.170090	2.170090
-0.5	2.614038	2.617403
0.01	3.007134	3.007133
0.5	3.336449	3.336449
2.0	4.167389	4.167389

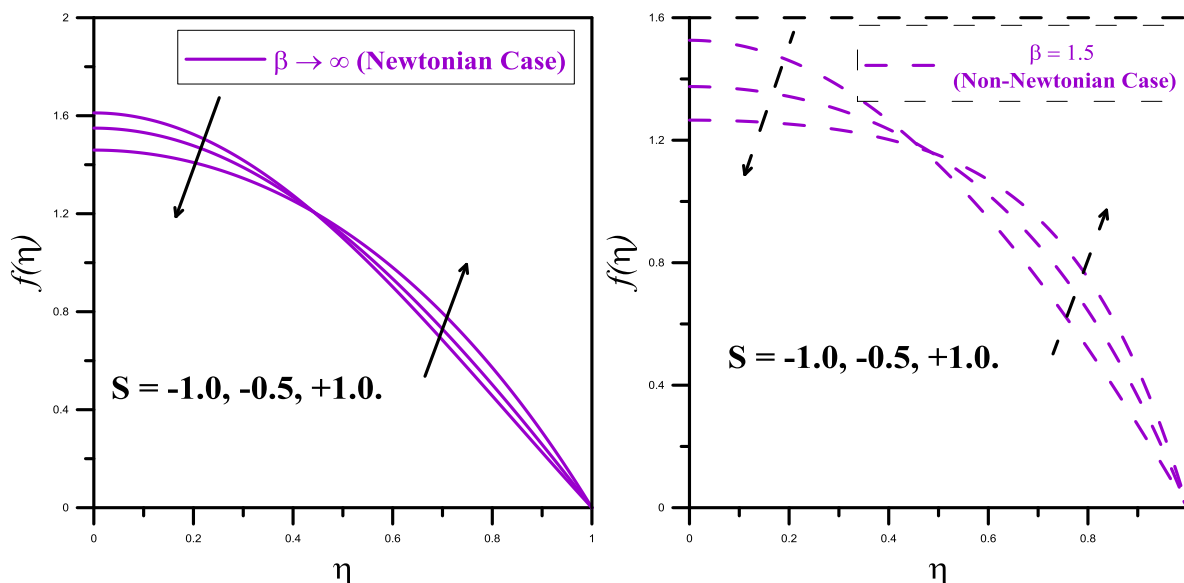


Fig. 2: Effect of  $S$  on  $f'(\eta)$

The influence of  $S$  on the temperature profile  $\theta(\eta)$  is explained in Figure 3 for both  $\beta = 1.5$  and  $\beta \rightarrow \infty$ . In this example,  $\theta(\eta)$  has a declining trend when  $S$  is increased, and it rapidly decreases when  $S$  is increased for both the fluid cases where  $\beta = 1.5$  and  $\beta \rightarrow \infty$ . From the physical point of view, the thickness of the thermal boundary layer upsurges for the absolute magnitude of the squeeze number due to the simultaneous movement of two plates. Physically, an enhancement of  $S$  has a significant effect on the velocity profile. When  $\eta$  is less than 0.5, the velocity in the squeezing flow increases because of a rise in the absolute value of  $S$ , whereas it decreases when  $\eta$  is greater than 0.5.

Moreover, the temperature profile is reduced when  $S$ 's magnitude increases. This is because the velocity profile decreases toward the lower plate as the distance between the dual plates gets smaller as the positive  $S$  values increase.

Figure 4 illustrates the significant influence of heat source or sink parameter  $Hs$  on temperature profile  $\theta(\eta)$ . For better values of  $Hs$ , in both scenarios ( $\beta = 0.5$  and  $\beta \rightarrow \infty$ ), the  $\theta(\eta)$  increases. Positive and negative indications of  $Hs$  correspond to the flow's heat generation and absorption, respectively. The energy released in the flow field during heat generation causes the temperature profile to improve.

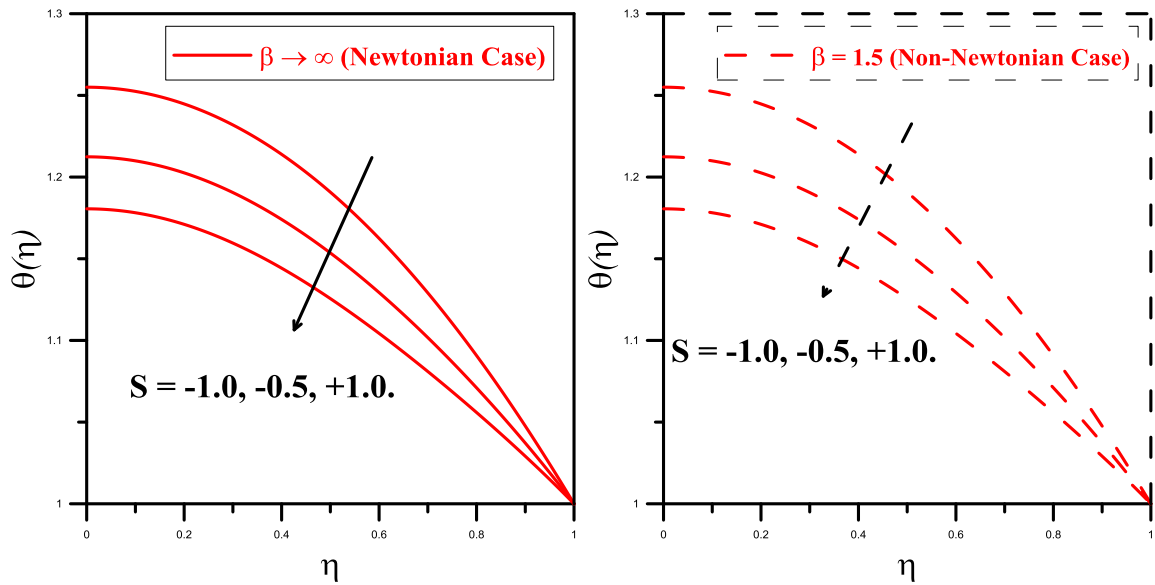


Fig. 3: Effect of  $S$  on  $\theta(\eta)$

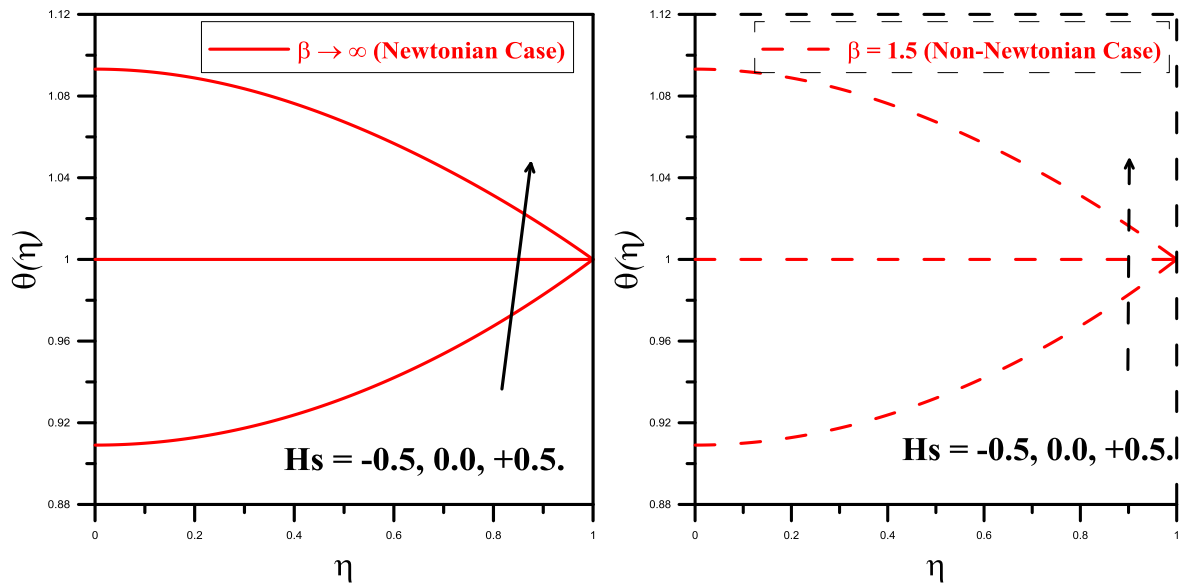


Fig. 4: Effect of  $H_s$  on  $\theta(\eta)$

The behavior of the concentration profile  $\phi(\eta)$  for increased values of  $S$  is shown in Figure 5 for both the scenarios when  $\beta = 1.5$  and  $\beta \rightarrow \infty$ . It reveals that with better values of  $S$ ,  $\phi(\eta)$  drops quickly. In Figure 6, the effect of  $\delta$  on  $\phi(\eta)$  is shown. This graph shows that for both  $\beta = 1.5$  and  $\beta \rightarrow \infty$ ,  $\phi(\eta)$  increases as  $\delta$  rises.

Figure 7 illustrates how  $\phi(\eta)$  behaves similarly for enlarged values of  $Sc$  in the scenarios when  $\beta = 1.5$  and  $\beta \rightarrow \infty$ .

Figure 8 shows the change in the solid volume fraction  $\varphi_2$  over  $f'(\eta)$ . The picture shows that when  $\eta > 0.5$ ,  $f'(\eta)$  increases for upgrading the solid volume percentage of  $\varphi_2$ , but  $f'(\eta)$  continues to decrease when  $\eta$  values drop from 0.5 to 0.

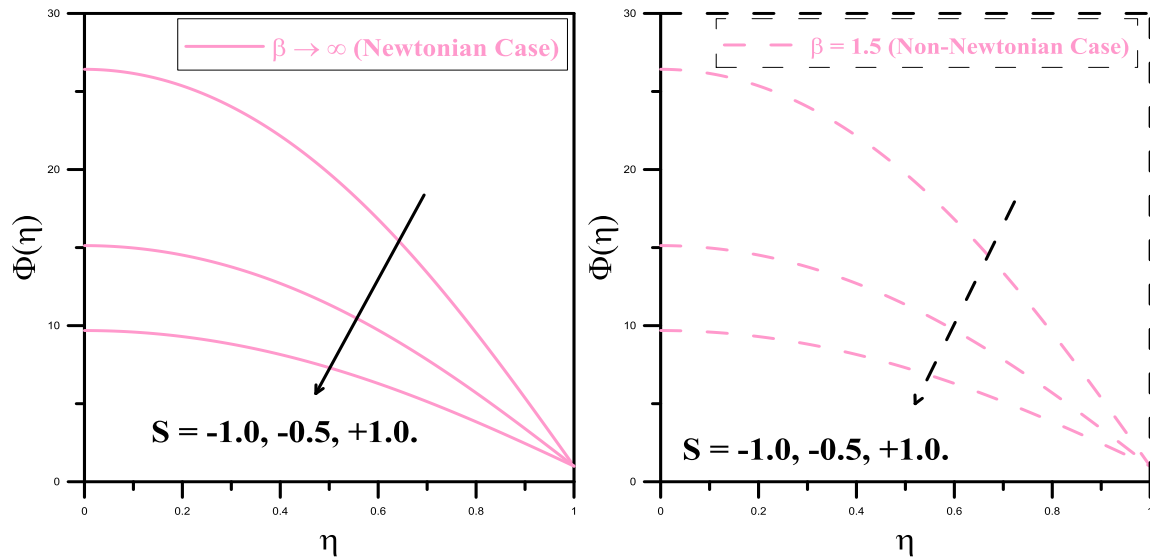


Fig. 5: Effect of  $S$  on  $\phi(\eta)$

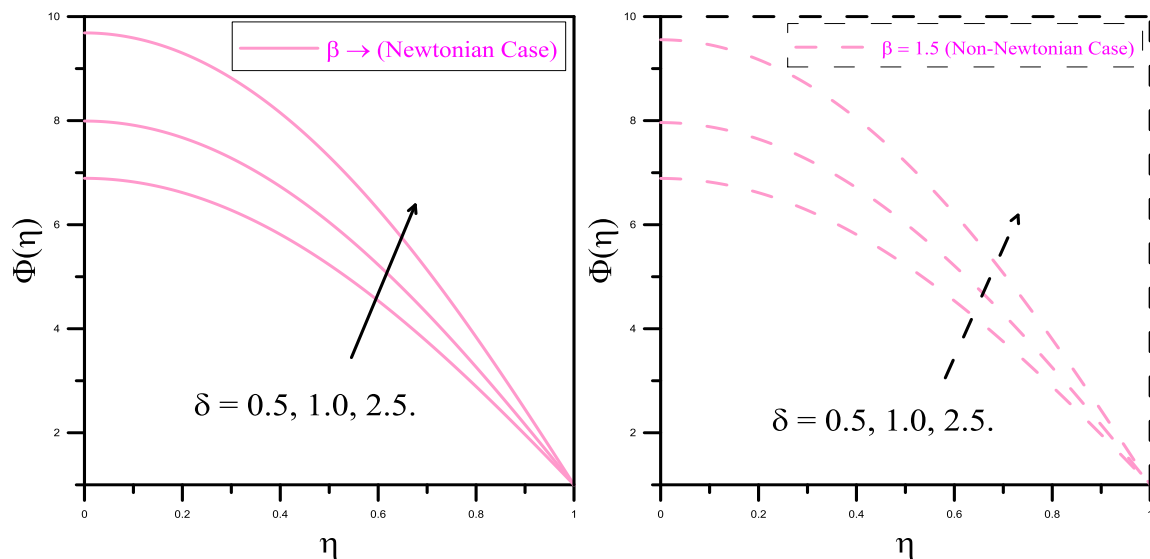


Fig. 6: Effect of  $\delta$  on  $\phi(\eta)$

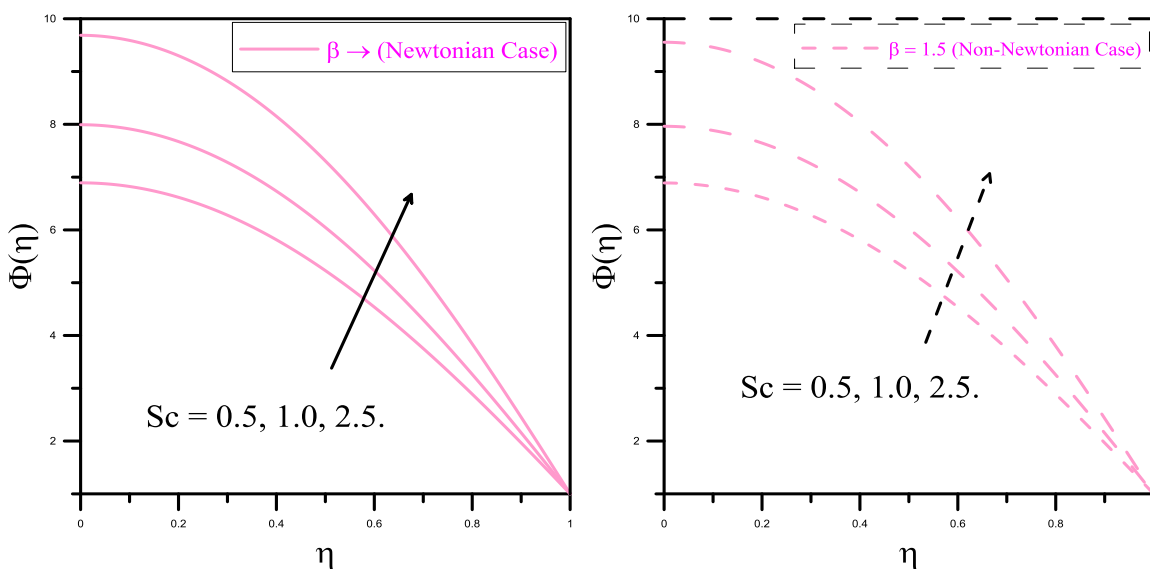


Fig. 7: Effect of  $Sc$  on  $\phi(\eta)$

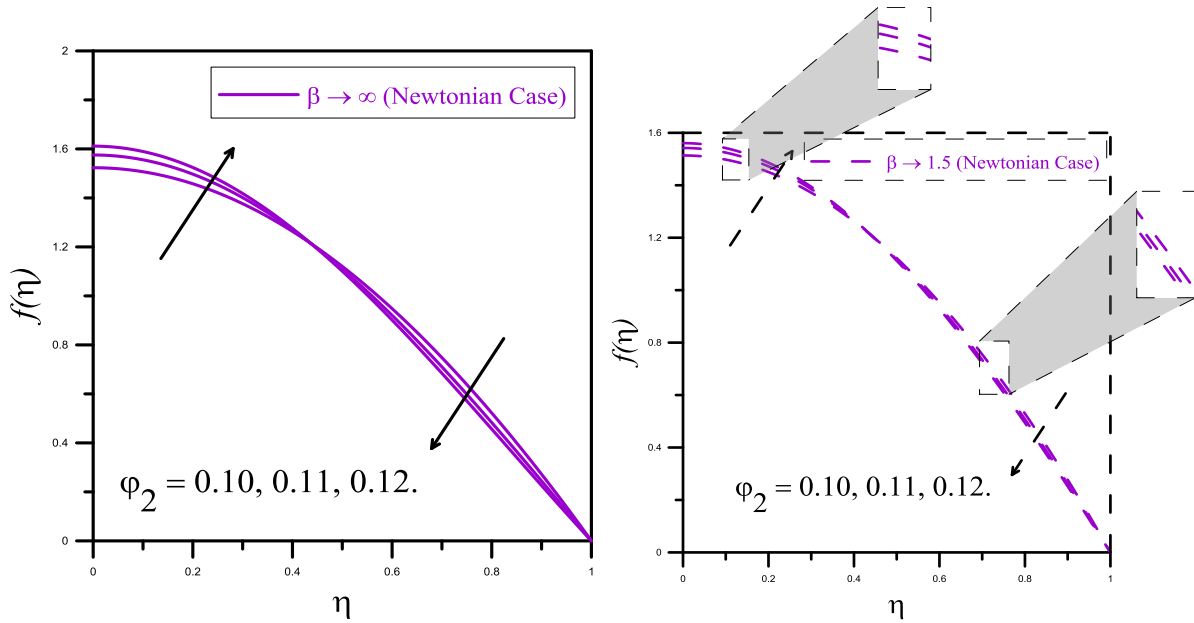


Fig. 8: Effect of  $\varphi_2$  on  $f(\eta)$

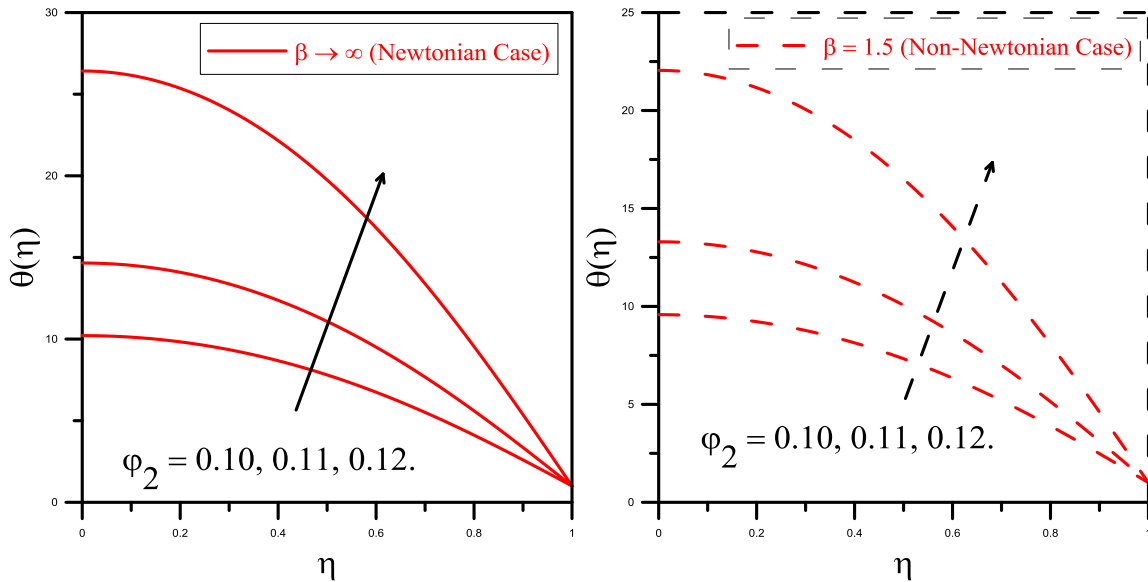


Fig. 9: Effect of  $\varphi_2$  on  $\theta(\eta)$

As the boundary layer thickness increases, the hybrid fluid's velocity increases when  $\beta \rightarrow \infty$  and decreases when  $\beta = 1.5$ , which corresponds to the Casson hybrid fluid. Figure 9 shows the change in the solid volume fraction  $\varphi_2$  over  $\theta(\eta)$ . The rate of heat transmission is accelerated by the addition of  $\varphi_2$ . Compared to other hybrid nanoliquids, Casson hybrid nanoliquid has a higher rate of heat transmission. Figure 10 shows the fluctuation of the solid volume fraction  $\varphi_2$  over  $\phi(\eta)$ . Because the Casson parameter has been added, the concentration in the Casson hybrid nanoliquid is higher than in the hybrid nanoliquid.

Table 3, Table 4 and Table 5 show the behavior of mass, heat, and momentum transport rates for

various values of the flow parameters. Table 3 shows that the momentum transport coefficient ( $-f''(1)$ ) rises when the plate is moving toward one another and falls when the plate is moving away from one another. It is also observed that the skin-friction coefficient near the wall lowers when the plates separate due to the increasing value of  $\beta$ . Table 4 provides an illustration of how physical characteristics affect the heat transfer rate ( $\theta'(1)$ ). Table 4 makes it evident that the Nusselt number rises as the squeezing number's magnifying values do. This results from the fluid in the channel being less viscous.

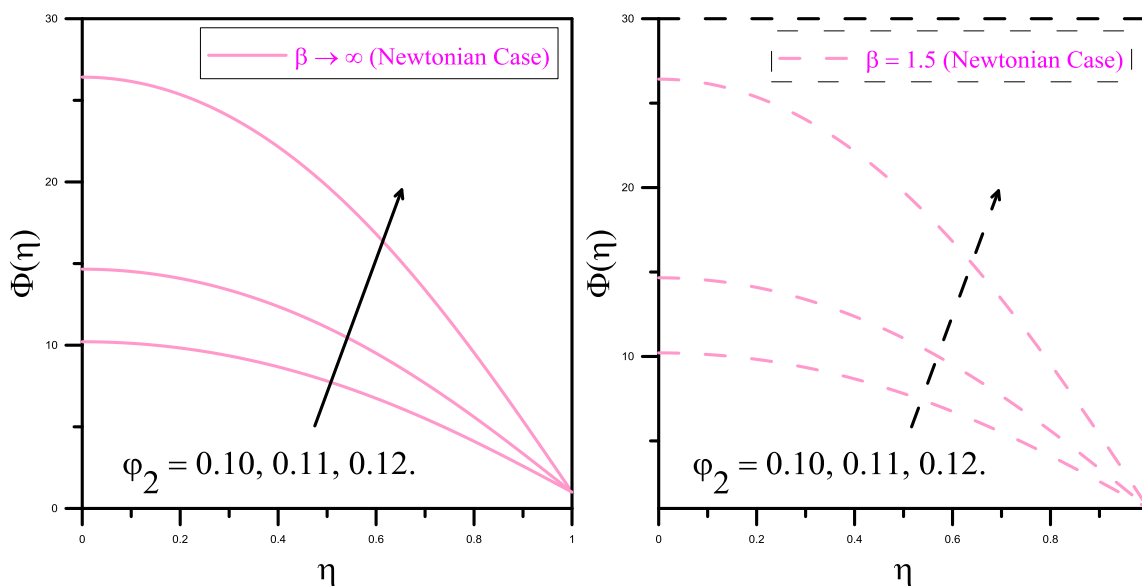


Fig. 10: Effect of  $\varphi_2$  on  $\Phi(\eta)$

Table 3. Local skin-friction coefficient for various values of  $S$  and  $\beta$

$S$	$\beta$	$\frac{-\left(1 + \frac{1}{\beta}\right) f''(1)}{(1 - \varphi_1)^{2.5} (1 - \varphi_2)^{2.5}}$
-1.50	3.00	4.732768497
-0.50		6.167692445
0.20		7.001042863
1.50		8.311880921
2.50		9.175911670
4.00		10.31304423
2.00	2.00	9.632617717
	2.50	9.107675851
	3.00	8.756605950
	3.50	8.505227354
	5.00	8.051288352

Table 4. Local Nusselt number coefficient for various values of  $S$  and  $Hs$

$S$	$Hs$	$-\frac{k_{hnf}}{k_f} \theta'(1)$
-0.30	0.10	0.1126336986
-0.10		0.1089894740
0.20		0.1039879097
0.50		0.0994707971
1.50		0.0871236816
2.00		0.20
	0.30	0.2771814053
	0.40	0.3953297053
	0.50	0.5323996434
	0.60	0.6943066029

Table 5. Local Sherwood number coefficient for various values of  $S$  and  $H_s$

$S$	$Sc$	$\delta$	$-(1 - \varphi_1)^{2.5}(1 - \varphi_2)^{2.5}\phi'(1)$
-0.30	0.50	1.50	1.842767138
-0.10			1.675170790
0.20			1.474330027
1.50			0.962905129
2.50			0.751230420
2.00	0.70		1.023652562
	0.80		1.072418601
	0.90		1.095900128
	0.91		1.096956906
	0.92		1.097791699
	0.50	-1.40	-0.903792841
		-0.50	-0.314212136
		1.50	0.845402744
		2.00	1.079439671
		2.50	1.280753231

In the same way, Table 5 shows how different control settings affect the mass transfer rate ( $\phi'(1)$ ) in the flow region. Table 5 demonstrates unequivocally that the mass transmission rate at the wall falls as  $S$  increases. The primary cause of this is the channel's construction. Additionally, it is observed that as  $Sc$  levels rise, mass transfer rate rises as well. Furthermore, because it is constructive, ( $\phi'(1)$ ) decreases for  $\delta > 0$  and grows for  $\delta < 0$ .

#### 4 Conclusion

The current study examines the flow behavior of a Casson hybrid nanofluid between two parallel plates under the influence of a heat source or sink and thermophoretic particle deposition. Appropriate similarity variables are used to convert the governing equations representing the fluid flow into nonlinear ODEs, which are then numerically solved using the RKF 45 method. Consequently, the effects of physical parameters on the distinct fluid profiles are depicted via graphs. The significant conclusions of the present inquiry are as follows:

- For both Casson hybrid nanofluid and conventional hybrid nanoliquid, fluid velocity decreases with increased squeezing number values for  $\eta < 0.5$  and increases for  $\eta > 0.5$ ; however, a reversal tendency is observed for varying local porosity parameter values.
- The temperature profile decreases as the squeezing number increases, but it increases for higher heat source/sink parameter values in

both the Casson hybrid nanofluid and hybrid nanoliquid situations.

- For both Casson hybrid nanofluid and ordinary hybrid nanoliquid, the concentration profile exhibits the opposite behavior with increased values of squeezing number, but it greatly improves with an increase in thermophoretic parameter and Schmidt number.
- An increase in the thermophoretic parameter over the Schmidt number causes the rate of mass transfer to accelerate.

#### References:

- [1] Choi SUS, Eastman J. Enhancing thermal conductivity of fluids with nanoparticles. 1995; 66.
- [2] Irfan M, Khan M, Khan WA, Alghamdi M, Ullah MZ. Influence of thermal-solutal stratifications and thermal aspects of non-linear radiation in stagnation point Oldroyd-B nanofluid flow. *Int Commun Heat Mass Transfer*.2020; 116:104636, <https://doi.org/10.1016/j.icheatmasstransfer.2020.104636>.
- [3] Kotresh MJ, Ramesh GK, Shashikala VKR, Prasannakumara BC. Assessment of Arrhenius activation energy in stretched flow of nanofluid over a rotating disc. *Heat Transfer*. 2021;50(3):2807-2828. <https://doi.org/10.1002/htj.22006>.
- [4] J.K. Madhukesh, R. Naveen Kumar, R.J. Punith Gowda, B.C. Prasannakumara, G.K. Ramesh, M. Ijaz Khan, Sami Ullah Khan,

- Yu-Ming Chu. Numerical simulation of AA7072- AA7075/ water-based hybrid nanofluid flow over a curved stretching sheet with Newtonian heating: a non-Fourier heat flux model approach. *J Mol Liq.* 2021; 335:116103, <https://doi.org/10.1016/j.molliq.2021.116103>.
- [5] Thriveni K, Mahanthesh B. Sensitivity analysis of nonlinear radiated heat transport of hybrid nanofluid in an annulus subjected to the nonlinear Boussinesq approximation. *J Therm Anal Calorim.* 2021;143(3): 2729-2748, <https://doi.org/10.1007/s10973-020-09596-w>.
- [6] Christopher AJ, Magesh N, Gowda RJP, Kumar RN, Kumar RSV. Hybrid nanofluid flow over a stretched cylinder with the impact of homogeneous–heterogeneous reactions and Cattaneo–Christov heat flux: Series solution and numerical simulation. *Heat Transfer.* 2021; 50(4):3800-3821, <https://doi.org/10.1002/htj.22052>.
- [7] Nadeem S, Abbas N, Malik MY. Inspection of hybrid based nanofluid flow over a curved surface. *Comput Methods Programs Biomed.* 2020; 189:105193, <https://doi.org/10.1016/j.cmpb.2019.105193>.
- [8] Mallikarjuna HB, Nirmala T, Gowda RJP, Manghat R, Kumar RSV. Two-dimensional Darcy–Forchheimer flow of a dusty hybrid nanofluid over a stretching sheet with viscous dissipation. *Heat Transfer.* 2021; 50(4): 3934-3947, <https://doi.org/10.1002/htj.22058>.
- [9] Hayat T, Sajjad R, Alsaedi A, Muhammad T, Ellahi R. On squeezed flow of couple stress nanofluid between two parallel plates. *Results Phys.* 2017; 7:553-561, <https://doi.org/10.1016/j.rinp.2016.12.038>.
- [10] Ijaz Khan M, Rahman M, Khan SA, Hayat T, Imran Khan M. Evaluation of entropy generation in cubic autocatalytic unsteady squeezing flow of nanofluid between two parallel plates. *Comput Methods Programs Biomed.* 2020; 185:105149, <https://doi.org/10.1016/j.cmpb.2019.105149>.
- [11] Garg VK, Jayaraj S. Thermophoretic deposition in crossflow over a cylinder. *J Thermophys.* 1990;4(1): 115-116, <https://doi.org/10.2514/3.29164>.
- [12] Chiou MC. Particle deposition from natural convection boundary layer flow onto an isothermal vertical cylinder. *Acta Mech.* 1998; 129(3):163-176, <https://doi.org/10.1007/BF01176743>.
- [13] Hafeez A, Khan M, Ahmed J. Oldroyd- B fluid flow over a rotating disk subject to Soret–Dufour effects and thermophoresis particle deposition. *Proc Inst Mech Eng C J Mech Eng Sci.* 2020:1-8, <https://doi.org/10.1177/0954406220946075>.
- [14] M. Mustafa, T. Hayat, S. Obaidat; On heat and mass transfer in the unsteady squeezing flow between parallel plates; *Mechanica*, 47 (2012), pp. 1581–1589, <https://doi.org/10.1007/s11012-012-9536-3>.

### Contribution of Individual Authors to the Creation of a Scientific Article (Ghostwriting Policy)

**A. EL Harfouf:** Conceptualization, Formal analysis, Investigation, Methodology, Project administration, Resources, Validation, Writing – original draft, Data curation, Software, Visualization.

**R. Herbazi:** Conceptualization, Formal analysis, Investigation, Methodology, Project administration, Resources, Validation, Writing – review & editing.

**W. Abouloifa:** Conceptualization, Investigation, Writing – review & editing. **H. Mes-adi:**

Conceptualization, Formal analysis, Investigation, Methodology, Project administration, Resources, Validation, Writing – review & editing. **A. Wakif:**

Conceptualization, Investigation, Project administration, Supervision, Writing – review & editing. **M. Mejdal:**

Conceptualization, Formal analysis, Investigation, Methodology, Project administration, Resources, Validation, Writing – review & editing. **M. Nfaoui:**

Conceptualization, Investigation, Project administration, Writing – review & editing. **S. Hayani Mounir:**

Conceptualization, Investigation, Project administration, Supervision, Writing – review & editing.

### Sources of Funding for Research Presented in a Scientific Article or Scientific Article Itself

No funding was received for conducting this study.

### Conflict of Interest

The authors have no conflicts of interest to declare.

### Creative Commons Attribution License 4.0 (Attribution 4.0 International, CC BY 4.0)

This article is published under the terms of the Creative Commons Attribution License 4.0

[https://creativecommons.org/licenses/by/4.0/deed.en\\_US](https://creativecommons.org/licenses/by/4.0/deed.en_US)